



1 **Peak river flows in cold regions – Drivers and modelling using GRACE satellite**

2 **observations and temperature data**

3 Shusen Wang<sup>1,\*</sup>, Fuqun Zhou<sup>1</sup>, Hazen A. J. Russell<sup>2</sup>, Ran Huang<sup>3</sup>, Yanjun Shen<sup>4</sup>

4 <sup>1</sup> Canada Centre for Remote Sensing, Natural Resources Canada, Ottawa, ON, Canada

5 <sup>2</sup> Geological Survey of Canada, Natural Resources Canada, Ottawa, ON, Canada

6 <sup>3</sup> College of Information & Electrical Engineering, China Agricultural University, Beijing, China

7 <sup>4</sup> Key Laboratory of Agricultural Water Resources, Chinese Academy of Sciences, Shijiazhuang,

8 China

9 **Running title: Forecasting peak river flows in cold regions**

10 \*Corresponding author:

11 560 Rochester Street, Ottawa, ON K1A 0E4, Canada

12 Phone: (613) 759-6462

13 E-mail: [Shusen.Wang@Canada.ca](mailto:Shusen.Wang@Canada.ca)

14



15 **Abstract**

16           The peak river flow for the Mackenzie River is modelled using GRACE satellite  
17 observations and temperature data, which advances the applications of space-based time-variable  
18 gravity measurements in cold region flood forecasting. The model estimates peak river flow by  
19 simulating peak surface runoff from snowmelt and the corresponding baseflow. The modelled  
20 results compared fairly well with the observed values at a downstream hydrometric station. The  
21 results also revealed an average 22-day travel time for the snowmelt water to reach the  
22 hydrometric station. The major driver for determining the peak flow was found to be the  
23 temperature variations. Compared with the Red River basin, the results showed that the  
24 Mackenzie River basin has relatively high water storage and water discharge capability, and low  
25 snowmelt efficiency per unit temperature. The study also provides a GRACE-based approach for  
26 basin-scale snowfall estimation, which is independent of in situ measurements and largely  
27 eliminates the limitations and uncertainties with traditional approaches. The model is relatively  
28 simple and only needs GRACE and temperature observations for peak flow or flood forecasting.  
29 The model can be readily applied to other cold region basins, and could be particularly useful for  
30 regions with minimal data.

31 **Key Points:**

- 32       • Peak runoff and winter baseflow are modelled using GRACE observations.
- 33       • Major drivers controlling peak river flows or floods in cold regions are identified.
- 34       • Mechanisms underlying peak flow regimes of different basins are discussed.
- 35       • GRACE observation is used for basin-scale snowfall estimate.

36



## 37 **1. Introduction**

38 Peak river flow and its forecasting are of considerable interest to flood control and  
39 emergency service agencies, river recreationists, wildlife managers, hydropower plant operators  
40 and anyone interested in the combined effect of watershed yield and human regulation on the  
41 river maximum flows at a site. Flooding is a hazard to developed areas and to human activities in  
42 the floodplain and causes human hardship and economic loss (International Joint Commission,  
43 2000; Burton et al., 2016). Flooding ranks as one of the most damaging forms of natural disasters  
44 in the world. On the other hand, flooding is essential to a healthy environment. Floods can  
45 benefit the natural environment and sustain many ecosystems. For instance, the recurrent  
46 inundation of the Peace-Athabasca Delta in the Mackenzie River basin in Canada has fostered an  
47 environment in which plant and animal life has achieved a balance dependent on flooding. In  
48 fact, water spilling across the floodplain nourishes the wetlands of many of Canada's major  
49 deltas (Andrews, 1993).

50 Peak river flow in cold regions is commonly a result of snowmelt during the spring  
51 break-up, or the subarctic nival regime (Church, 1974). During the winter most of the  
52 precipitation is in the form of snow, which accumulates in the basins until the spring breakup.  
53 Depending on the temperature in the spring freshet, huge quantities of water from snowmelt can  
54 be produced. Meltwater is unable to penetrate when the ground is frozen and runs off over the  
55 ground surface into rivers and lakes, resulting in peak flows and floods. Snowmelt runoff floods  
56 are the most common type of flooding in Canada (Andrews, 1993; Yang et al., 2009; Rannie,  
57 2015; Wang and Russell, 2016).

58 Two key factors determining the magnitude of peak river flows or floods during the  
59 freshet are the amount of snow water equivalent (SWE) available at the time of spring breakup



60 and the temporal patterns of rising air temperature during the snowmelt season. As such,  
61 forecasting peak flows or floods for rivers in cold regions, regardless of the methods being used,  
62 heavily relies on information for basin-scale SWE and temperature. SWE can be estimated by  
63 the difference of snowfall and water loss from snow sublimation. Unfortunately, accurately  
64 measuring snowfall is difficult and often involves large uncertainties. Studies show that the  
65 measurement errors of snowfall at climate stations can be as high as 50% due to the wind-  
66 induced undercatch and the fact that many trace events cannot be easily measured (Goodison et  
67 al., 1998). Snow sublimation estimation is also difficult and has large uncertainties (Wang et al.,  
68 2013; Wang et al., 2015a). In addition, cold regions commonly have very sparse observational  
69 data. For instance, the density of climate stations in the Canadian Northwest Territory is only  
70 about 2 stations per 100,000 km<sup>2</sup> (Metcalf, 1994). This sparse spatial density of stations makes  
71 the up-scaling of SWE from site to basin-scale extremely difficult and unreliable. Remote  
72 sensing, either by optical (e.g., Hall et al., 2002) or microwave (e.g., Dong et al., 2005) satellite  
73 sensors, can provide valuable information for the spatial snow cover distribution. However,  
74 remote sensing approaches for the estimation of SWE depend on retrieving snow parameters  
75 such as snow cover area, snowpack depth, density, liquid and ice content, etc., which can be  
76 significantly affected by the climate/atmosphere and land surface/snowpack conditions, such as  
77 the temperature effect on snow density, and cloud, vegetation cover and topographic impacts on  
78 snow cover area identification (Nolin, 2010). Moreover, SWE models from remote sensing  
79 heavily rely on in situ data for calibration and validation, which may propagate the errors in the  
80 in situ measurements to the remote sensing products (Hall and Riggs, 2007). Due to the  
81 difficulties mentioned above, spatial snow data products either from traditional methods or from  
82 remote sensing approaches often have large uncertainties. For instance, recent studies have found



83 that errors in snow data are the principal contribution to the water budget imbalance in cold-  
84 region basins (Wang et al., 2014a; Wang et al., 2014b; Wang et al., 2015b). Consequently,  
85 accurate estimation of basin-scale SWE is a key challenge in improving flood forecasting over  
86 cold region rivers.

87 In a recent study, Wang and Russell (2016) developed a flood forecasting model using  
88 the Gravity Recovery and Climate Experiment (GRACE) satellite observations and temperature  
89 data. In the model, the total water storage (TWS) data from GRACE was used to estimate the  
90 basin-scale SWE at the spring breakup. The model does not require snowfall and sublimation  
91 data as well as the site-to-basin upscaling process, thus largely eliminating the data constraints  
92 discussed above. In Wang and Russell (2016), the model was applied to the Red River basin, a  
93 USA-Canada transboundary watershed located in central North America, mostly in the U.S.  
94 states of Minnesota and North Dakota. Floods predicted by the model compared well with the  
95 observed values. However, the Red River has a drainage area of 116,500 km<sup>2</sup>, which is limited in  
96 size relative to the large footprint of the GRACE satellites. This size limitation may contribute to  
97 the large data uncertainties in the TWS of the basin which might substantially impact the  
98 accuracy of flood forecasts. Second, a conclusion found in Wang and Russell (2016) is that the  
99 SWE at the spring breakup is the major driver determining the magnitudes of peak river flows,  
100 with temperature playing the secondary role. Whether this conclusion is valid for other basins  
101 with different hydroclimatic conditions still remains to be investigated.

102 In this study, the model of Wang and Russell (2016) is calibrated to forecast the peak  
103 flows for the Mackenzie River in Canada (Fig. 1). The Mackenzie River basin has a large  
104 drainage area of 1.8 million square kilometres, which largely eliminates the constraints imposed  
105 by the large footprint of GRACE. The basin is located in northwest Canada, about 18 degrees of



106 latitude north of the Red River basin. Compared with the Red River basin, the Mackenzie River  
107 basin has very different physiographic and hydroclimatic conditions, including the very low  
108 temperature, large amount but small interannual variations in winter snowfall, as well as high  
109 water storage conditions. As a result, the Mackenzie River has much delayed peak discharge  
110 flows that have much smaller interannual variations than the Red River. The objective of this  
111 study is to evaluate the model performance in forecasting, and to identify the major drivers in  
112 determining, the peak flows or floods for the Mackenzie River. The model results and parameter  
113 values will be compared with that for the Red River to help better understand the mechanisms  
114 underlying the peak river flows for basins with different physiographic and hydroclimatic  
115 conditions.

## 116 **2. Study Region, Data, and Hydroclimate Characterization**

117 The Mackenzie River Basin is one of the largest North American river basins and covers  
118 about 1.8 million square kilometres or about 20% of the landmass of Canada. Our basin study  
119 area is located between 52° to 70° N and encompasses three major geographical regions. In  
120 the west, the Western Cordillera consists of a series of mountain chains and valleys or high  
121 plateaus. Many ridges of the Rocky Mountain chain exceed 2000 m elevation, and some have  
122 glaciers occupying the mountain tops and high valleys. To the east is the Canadian Shield, a  
123 rolling terrain with myriad of lakes and valley-wetlands separating upland outcrops of  
124 Precambrian bedrock. The central zone is part of the Interior Plains, with wetlands, lakes, and  
125 vegetation that ranges from prairie grassland in the south, through the boreal and subarctic  
126 forests, to the tundra in the north (Woo and Thorne, 2003). There are a large number of lakes  
127 across the basin, with the top three large lakes (i.e., Great Bear Lake, Great Slave Lake and Lake  
128 Athabasca) having a total surface area of over 67,000 km<sup>2</sup>. The basin has a wetland coverage of



129 approximately 49% and permafrost underlies approximately 75%. The Mackenzie River system  
130 flows a total of 4,241 kilometres from its headwaters northwards to the Arctic Ocean.

131 The data required by the model for peak flow estimation includes GRACE TWS and  
132 daily temperature  $T_a$ . The in situ measurement of river flow  $Q$  is used for model calibration. The  
133 GRACE Release-05 TWS datasets were downloaded from the GRACE Tellus website  
134 ([ftp://podaac-ftp.jpl.nasa.gov/allData/tellus/L3/land\\_mass/RL05/](ftp://podaac-ftp.jpl.nasa.gov/allData/tellus/L3/land_mass/RL05/)) (Swenson, 2012). The datasets  
135 include monthly TWS from three data processing centers: CSR (University of Texas/Center for  
136 Space Research), GFZ (GeoForschungsZentrum Potsdam), and JPL (Jet Propulsion Laboratory).  
137 The data are provided in a spatial sampling of 1 degree grids in both latitude and longitude. The  
138 land grid scale factor, as provided with the TWS data, was applied to recover signal loss due to  
139 filtering and truncation (Swenson and Wahr, 2006). Monthly error estimates in the GRACE  
140 TWS for the Mackenzie River Basin are based on combined measurement and leakage error,  
141 following Wahr et al. (2006). A detailed description of the data processing and accuracy  
142 assessment can be found in Landerer and Swenson (2012). The differences among the three  
143 datasets, as shown later, were found to be small over our study region. In this study, the average  
144 TWS of the three datasets was used. The study covers 12 snow-years from the fall of 2002 to the  
145 spring of 2014. The baseline of the TWS, which was based on the average from January 2004  
146 through December 2009 in the original data, was re-adjusted to the minimum value found over  
147 the 12-year period.

148 The basin average  $T_a$  was calculated from the Global Land Data Assimilation System  
149 (GLDAS) meteorological forcing of temperature, which is provided at a 3 hour time step and a  
150 spatial resolution of 0.25×0.25 degree latitude/longitude. The air temperature time series for  
151 2002-2014 was downloaded from Goddard Earth Sciences Data and Information Service Center



152 (<http://mirador.gsfc.nasa.gov/>). The daily air temperature of the grids is taken as the average of  
153 the 8 readings of the day, and the daily  $T_a$  of the basin is the average of the daily values of all the  
154 GLDAS grids within the basin. The GLDAS precipitation is also processed to assist our  
155 discussion. The daily precipitation of each grid is the sum of the 8 readings of the day, and the  
156 daily value of the basin is the average of all the grids within the basin.

157         The in situ daily  $Q$  observed at the hydrometric station of Mackenzie River at Arctic Red  
158 River (station ID: 10LC014, Latitude: 67° 27' 21" N, Longitude: 133° 45' 11" W) was obtained  
159 from the Water Survey of Canada (<http://www.ec.gc.ca/rhc-wsc/>). The  $Q$  collected at this  
160 location, before the river branches into many distributaries, is considered as the total flow for the  
161 Mackenzie River system. The station controls an area of 1,679,100 km<sup>2</sup> (> 90% of the basin).  
162 The original  $Q$  is in m<sup>3</sup> s<sup>-1</sup> and it was converted to water depth (mm) using the basin area. The  
163 peak flow is the maximum mean daily flow (the highest average flow for an entire day) in a year  
164 at the station. It is worth noting that the  $Q$  data is only required for model calibration. The peak  
165 flow estimation, once the model is calibrated, will only need TWS and  $T_a$  prior to winter and at  
166 the snowmelt season in spring.

167         The Mackenzie River Basin has several climatic regions, including cold temperate,  
168 mountain, subarctic, and arctic zones. According to the climate data used in this study, the daily  
169  $T_a$  averaged for the basin ranged from a low of -36 °C to a high of 21 °C during the 12 study  
170 years (Fig. 2). The 12-year average  $T_a$  of the basin varied from -22.6 °C in winter to 16.4 °C in  
171 summer, with an annual mean of -2.4 °C. The temperature dropped below 0 °C in mid-October  
172 and rises above 0 °C at the end of April, with an annual average of more than 200 days having  
173 temperatures below 0 °C. In winter, the basin is in a deep frozen state and precipitation as  
174 snowfall accumulates until spring breakup. Annual precipitation over the 12 years ranged from a





175 low of 311 mm to a high of 432 mm, with an average of 386 mm (Fig. 2). Annual precipitation  
176 during the winter time when  $T_a < 0$  °C ranged from 124 mm to 189 mm, of which the average was  
177 157 mm, or 41% of the total annual precipitation. However, it is generally recognized that  
178 snowfall from the climate station measurements is underestimated. This will be further discussed  
179 using our GRACE-based estimates in Section 4.

180 The TWS of the basin has strong seasonal variations, with highest values around April  
181 before snow breakup and lowest values around October before snow starts to accumulate (Fig.  
182 2). The average seasonal variation range (peak to peak) for the 12 years was 116 mm. The  
183 pronounced seasonal pattern is mainly a result of snow accumulation combined with extremely  
184 low evapotranspiration and river discharge in winter, and high evapotranspiration combined with  
185 high river discharge in summer (Wang and Li, 2016). The TWS has moderate interannual  
186 variations. Among the 12 years, the maximum differences reached 68 mm in April and 77 mm in  
187 October. The three original TWS datasets have an average difference of 5.4 mm, which is minor  
188 compared with the seasonal variations of TWS for the basin. The combined measurement and  
189 leakage error for the GRACE TWS datasets is estimated at 9.9 mm, which is about 8.5 % of the  
190 average seasonal variation of TWS.

191 River flow of the Mackenzie River is greatest in spring when snowmelt occurs (Fig. 2).  
192 The peak flows for the study period observed at the station 10LC014 varied from a low of 24,200  
193  $\text{m}^3 \text{s}^{-1}$  in 2010 to a high of 35,000  $\text{m}^3 \text{s}^{-1}$  in 2013 (Fig. 2). The 12-year average peak flow was  
194 28,400  $\text{m}^3 \text{s}^{-1}$ . The date when peak river flow occurred was on June 3 on average, with the  
195 earliest on May 15 in 2005 and latest on July 12 in 2007. In the climate change context, studies  
196 have showed that the Mackenzie River is experiencing a shift of peak flows to earlier in the  
197 spring due to earlier melt of snow cover and river ice breakup (Prowse et al., 2010; Woo and



198 Thorne, 2003; Yang et al., 2014). The basin discharge in winter gradually decreases and at the  
199 time of spring breakup, the observed 12-year average flow was around  $3,700 \text{ m}^3 \text{ s}^{-1}$ . In summer,  
200 although the total amount of rain was higher than the winter snowfall, the river discharge peaks  
201 were significantly lower (Fig. 2), mainly due to the high evapotranspiration, recharge of water to  
202 the soil and aquifers, and relatively even distribution of rain over the season. The large lakes in  
203 the basin also provide natural regulation to the system.

### 204 3. Methods

#### 205 3.1. Model Description

206 The model includes five major steps that are summarised below.

##### 207 Step 1: Determining snow season and the total water storage change

208 This study only concerns the snow season, defined as the time period from the start ( $t_0$ ) of  
209 snow accumulation in late autumn to the snow breakup ( $t_b$ ) in the next spring (Fig. 3). The  $t_0$  is  
210 determined by the criteria of (1) the first precipitation event in late fall when daily average  
211 temperature  $T_a$  drops below  $0^\circ\text{C}$  and (2) the accumulated  $T_a$  after this date remains negative. The  
212 criteria are to ensure that precipitation is in the form of snow and to exclude temporary snowfalls  
213 that are likely to melt in early winter. After this date, the net snow amount, i.e., snowfall minus  
214 snow sublimation, is accumulated over the basin in winter during which the  $T_a$  remains far below  
215  $0^\circ\text{C}$  (Fig. 2). The spring breakup time  $t_b$  is determined by the criteria of (1) daily average  
216 temperature  $T_a$  rises above  $0^\circ\text{C}$  and (2) the accumulated  $T_a$  after this date remains positive. The  
217 criteria are to ensure that the heat conditions of the basin will lead to the spring breakup and to  
218 exclude the possible minor snowmelt events in the snow cover season in case the  $T_a$  momentarily  
219 rises above  $0^\circ\text{C}$ .



220 The basin total water storages at  $t_0$  and  $t_b$ , i.e.,  $TWS_0$  and  $TWS_b$ , are estimated by linearly  
 221 interpolating the GRACE TWS for the two months before and after  $t_0$  and  $t_b$ , respectively. The  
 222  $TWS_0$  represents the maximum amount of non-snow water in the basin during the snow cover  
 223 season. It mainly consists of surface water, soil water, and groundwater, part of which will be  
 224 discharged in winter. The  $TWS_b$  represents the sum of net snow accumulation ( $S_b$ ) and non-snow  
 225 water content left in the basin at time  $t_b$  (Fig. 3).

## 226 Step 2: Modelling baseflow

227 In winter due to the frozen soil and snow cover, water infiltration and evaporation at the  
 228 soil surface is minimal. The decrease of non-snow water ( $W$ ) in the basin,  $dW(t)/dt$ , is thus  
 229 mainly due to basin discharge or baseflow. In this study, the winter baseflow  $Q_{base}$  is modelled  
 230 using a first order differential equation:

$$231 \quad Q_{base}(t) = -dW(t)/dt = a(W(t) - b) \quad (1)$$

232 where  $a$  is a parameter representing the lump conductivity of the basin for water discharge, and  $b$   
 233 is a parameter representing the threshold value of  $W$  at which the basin would have zero  
 234 discharge. This simplified model represents the basin water discharge as proportional to the  
 235 available water storage and lump basin conductivity for discharge.

236 With the above model and the initial condition of  $W(t_0) = TWS_0$ , the accumulated total  
 237 baseflow in winter,  $Q_{sum}$ , can be determined by:

$$238 \quad Q_{sum} = \int_{t_0}^{t_b} Q_{base}(t) dt = TWS_0 - (TWS_0 - b)e^{-a(t_b - t_0)} - b \quad (2)$$



239 The values for parameters  $a$  and  $b$  are obtained numerically by finding the least square errors  
 240 between the observed and modelled  $Q_{sum}$  for the 12 study years. Once  $a$  and  $b$  are known, the  
 241 baseflow rate at any time from  $t_0$  can be calculated as:

$$242 \quad Q_{base}(t) = a(TWS_0 - b)e^{-at}. \quad (3)$$

### 243 **Step 3: Determining snow water equivalent at spring break-up time**

244 After  $Q_{sum}$  (Eq. 2) is known, the snow water equivalent at  $t_b$ ,  $S_b$ , can then be obtained as  
 245 the sum of  $Q_{sum}$  and the change of TWS in the snow season (i.e.,  $TWS_b - TWS_0$ ) based on water  
 246 balance of the basin (Fig. 3):

$$247 \quad S_b = TWS_b - TWS_0 + Q_{sum} \quad (4)$$

248 The  $S_b$  represents the initial amount of snow which is going to melt following the  
 249 temporal trajectory of air temperature as described next. Note that snow sublimation in winter is  
 250 implicitly included in the estimate of  $S_b$  as GRACE measures the net change of water storage,  
 251 which is contributed by the difference of snowfall and snow sublimation in winter.

### 252 **Step 4: Modelling snowmelt ( $M$ ) and peak surface runoff ( $Q_{runoff}$ )**

253 The snowmelt is estimated by a temperature index model at a daily time step:

$$254 \quad M(t) = \min(S(t), \alpha(T_a(t) - \beta)) \quad (5)$$

255 where  $M(t)$  and  $S(t)$  is the snowmelt and snow amount available on day  $t$  (Note  $S(t) = S(t-1) - M(t-1)$ ),  
 256 respectively,  $\beta$  is a base temperature for snowmelt and  $\alpha$  is the snowmelt rate per unit of  
 257 temperature above  $\beta$ . Equation (5) determines the actual snowmelt rate by both temperature and  
 258 snow availability on a given date. The time series of snowmelt is calculated using the initial



259 condition of  $S_b$  (Fig. 3) and the daily  $T_a$  time series. The parameter values for  $\alpha$  and  $\beta$  were  
260 solved using a nested numerical iteration scheme to find the best correlation between peak  
261 snowmelt rate and the observed peak surface runoff. Observed peak surface runoff is calculated  
262 as the difference between observed peak river flow and the corresponding baseflow obtained  
263 using Equation (3). The model for estimating peak surface runoff,  $Q_{runoff}$ , from peak snowmelt is  
264 obtained after this numerical process is done.

### 265 **Step 5: Modelling peak river flow**

266 The modelled peak river flow is the sum of peak surface runoff and the corresponding  
267 baseflow obtained above:

$$268 \quad Q_{peak} = Q_{base} + Q_{runoff} \quad (6)$$

269 In summary, the model determines peak river flows by simulating its two components of  
270 peak surface runoff from snowmelt and the corresponding baseflow from basin discharge. The  
271 snowmelt is simulated by a temperature index model. The basin discharge is simulated by a first  
272 order differential equation model. There is a total of four parameters,  $a$  and  $b$ , which are  
273 calibrated using the total winter flow, and  $\alpha$  and  $\beta$ , which are calibrated using the observed peak  
274 surface runoff. Once calibrated, the model only needs GRACE TWS and  $T_a$  as inputs for  
275 determining peak river flow after spring breakup.

### 276 **3.2. Model Evaluation**

277 The model results were compared to in situ  $Q$  observations and evaluated using mean  
278 absolute error ( $MAE$ ), the Pearson correlation coefficient ( $r$ ) and t-test for significance levels ( $p$ ),  
279 as well as the Nash–Sutcliffe model efficiency coefficient ( $E$ ). The  $E$  is commonly used to assess



280 the predictive power of hydrological models. The leave-one-out cross-validation (LOO-CV)  
281 approach is used to evaluate the general model performance in peak river flow forecasting. The  
282 result from this LOO-CV evaluation is generally a more conservative estimate of the model  
283 performance than that trained on all samples. The model results were also compared with other  
284 basins to understand the mechanisms underlying the variations of peak flows over different  
285 regions.

#### 286 **4. Results and Discussion**

287 The model gives an average estimate for the start of snow cover of  $t_0$  on October 14 and  
288 spring breakup of  $t_b$  on April 29. The average snow water equivalent accumulated during this  
289 time period (197 days) is  $S_b=160$  mm. Given a water loss of 22 mm due to snow sublimation  
290 based on Wang et al. (2015a), the total snowfall during this time period from  $t_0$  to  $t_b$  is thus 182  
291 mm. In comparison, the corresponding total precipitation amount from the GLDAS datasets as  
292 discussed in Section 2 is 150 mm (snowfall=133 mm, rain=17 mm), which is about 20% lower  
293 than the GRACE-based estimate. Underestimation in snowfall over cold regions has been  
294 recognised by many studies (e.g., Wang et al., 2014a; Wang et al., 2015b) due to the errors as  
295 discussed in the Introduction section. This is particularly so for our study region as the available  
296 benchmark measurements, while extremely sparse, are mostly located in valleys or lowlands  
297 where the data are likely to underestimate the average condition of the entire basin. Many efforts  
298 have been made to correct the biases (e.g., Woo et al., 1983; Yang et al., 2005) but they are  
299 largely constrained by the difficulties in quantifying snow amounts at basin-scale. Our study  
300 provides a new GRACE-based approach for estimating snowfall at basin-scale. The approach is  
301 largely independent of in situ snowfall data thus eliminates most of the limitations and  
302 uncertainties in the snow gauge measurements and the site-to-basin up-scaling processes.



303           The model results show that the basin has a lump conductivity of  $a=1.07\times 10^{-3}$  day<sup>-1</sup> for  
304 water discharge, and a threshold value of  $b=-195.9$  mm of water below which the basin would  
305 have no discharge (Table 1). Compared with the Red River basin (Wang and Russell, 2016)  
306 which has  $a=0.49\times 10^{-3}$  day<sup>-1</sup> and  $b=9.2$  mm, the model results suggest that the Mackenzie River  
307 basin has a relatively high basin conductivity and high water storage state. This is consistent with  
308 the facts that the Mackenzie River basin has about 49% of its area as wetland and a large number  
309 of lakes which are highly effective in providing large storage capacities and are available for  
310 water discharge. Annual evapotranspiration for the basin is less than 60% of its annual  
311 precipitation (Wang et al., 2015a), so the basin has a large water surplus for soil and aquifer  
312 recharge as well as lake and wetland replenishment to sustain the winter low flows. In contrast,  
313 the Red River basin has a very flat terrain (the slope of the river averages less than 10 cm per  
314 kilometer). It also has high evapotranspiration that is close to its precipitation in summer,  
315 resulting in a very low water storage state prior to winter. The model results are also agreeable  
316 with the observed difference in winter flows, which are as low as 5.8 mm day<sup>-1</sup> for the Red River  
317 and as high as 48.8 mm day<sup>-1</sup> for the Mackenzie River as discussed next.

318           The model performance for winter baseflow estimation is shown in Table 1 and Fig. 4A.  
319 Compared to the mean observed baseflow of 48.8 mm in winter over the study period, the model  
320 has a mean absolute error of  $MAE=2.37$  mm, or 4.9% of the observed value. The modelled  
321 winter baseflow for the 12 years has a correlation coefficient of  $r=0.73$  with the observed values  
322 at a significance level of  $p<0.007$ . The Nash–Sutcliffe model efficiency coefficient for baseflow  
323 estimates is  $E=0.53$ . The results suggest that the basin winter discharge is primarily driven by its  
324 water storage prior to winter. Indeed, surface runoff is minimal in winter due to the lack of liquid  
325 precipitation. Water exchange between soil and groundwater is also minimal due to the frozen



326 soil. River flow in winter is thus sustained by groundwater and lake discharge that is controlled  
327 by pre-winter storage conditions. Determining groundwater and lake water storage at the basin  
328 scale is extremely difficult by traditional methods. The above results underscore the advantages  
329 of using GRACE satellite observations in estimating basin water storages and discharge in  
330 winter.

331 The snowmelt model suggests a snowmelt rate of  $\alpha=17.0$  mm per unit of temperature  
332 above a base temperature of  $\beta=2.1^{\circ}\text{C}$  (Table 2) for the Mackenzie River basin. The results are  
333 close to that obtained for the Red River basin which has  $\alpha=18.2$  mm  $^{\circ}\text{C}^{-1}$  and  $\beta=1.0^{\circ}\text{C}$  (Wang  
334 and Russell, 2016). The slightly higher melting power for a unit temperature with a lower base  
335 temperature for the Red River basin reflects the impacts of other environmental variables on the  
336 snowmelt, such as higher solar radiation for the Red River basin than for the Mackenzie River  
337 basin. Comprehensive and physically based snowmelt models are available and they have the  
338 advantages of simulating the integrated impact of all environmental variables (e.g., radiation,  
339 humidity, wind speed) on the snowmelt processes (e.g., Wang et al., 2007; Wang, 2008; Zhang et  
340 al., 2008), but these kinds of models are data demanding and difficult to implement for  
341 operational use over data scarce regions. We use the temperature index model as it needs  
342 minimal data input and is computationally simple. Our results also show that the temperature  
343 index model performs fairly well, consistent with many other studies (e.g., Li and Simonovic,  
344 2002; Griessinger et al., 2016).

345 The model performance for estimating peak surface runoff  $Q_{runoff}$  is shown in Table 2 and  
346 Fig. 4B. Compared with the observed mean  $Q_{runoff}$  of  $1.26$  mm  $\text{day}^{-1}$  over the study period, the  
347 model has a mean absolute error of  $MAE=0.1$  mm  $\text{day}^{-1}$ , or 7.6% of the observed value. The  
348 modelled  $Q_{runoff}$  for the 12 years has a correlation coefficient of  $r=0.82$  with the observed values





349 at a significance level of  $p < 0.001$ . The Nash–Sutcliffe model efficiency coefficient for surface  
350 runoff estimates is  $E = 0.50$ , slightly lower than that for the baseflow estimates.

351 To further determine the relative importance of  $T_a$  and  $S_b$  in  $Q_{runoff}$ , we analysed the  
352 relationship between  $S_b$  and  $Q_{runoff}$  (Fig. 5) and found that  $Q_{runoff}$  showed little correlation with  $S_b$ .  
353 The result indicates that total snow amount at spring breakup has little impact on the  $Q_{runoff}$ . As  
354 such, the rising temperature during the snowmelt season is the main driver for determining the  
355  $Q_{runoff}$  for the Mackenzie River basin. In contrast, the correlation between  $S_b$  and  $Q_{runoff}$  for the  
356 Red River basin was found to be fairly strong (Fig. 5). Specifically, without including  $T_a$ , the  $S_b$   
357 by itself explained more than two thirds (the coefficient of determination  $r^2 = 0.673$ ) of the  
358 interannual variations in  $Q_{runoff}$ , suggesting that the major driver for  $Q_{runoff}$  is  $S_b$  for the Red River  
359 basin (Wang and Russell, 2016). In another study by B.C. Ministry of Forests, Lands and Natural  
360 Resource Operations (2012), the peak flows for the Lower Fraser River were analysed. The  
361 Lower Fraser River is located in the latitudes between the Mackenzie River basin and the Red  
362 River basin. It was reported that the snow factor contributes about 20-40%, and the weather  
363 factors (mainly temperature) contribute about 60-80% to the flood risk. The above results for the  
364 three basins are consistent and appear to suggest that the principal drivers for peak river flows  
365 vary between basins. For northern basins temperature plays an important role, whereas for more  
366 southern basins the amount of snow accumulation is more important.

367 The difference in the main drivers for  $Q_{runoff}$  for the basins is largely due to the difference  
368 in their hydroclimatic conditions. The Red River basin has a mean snow accumulation at spring  
369 breakup of  $S_b = 73.3$  mm, which is less than half the accumulation for the Mackenzie River basin  
370 ( $S_b = 160.0$  mm). On the other hand, the Red River basin has a much larger interannual variations  
371 of  $S_b$  than that for the Mackenzie River basin. The coefficient of variation (CV) of  $S_b$ , or relative



372 standard deviation (RSD), which is calculated as the ratio of one standard deviation to the mean,  
373 is as high as 49.2% for the Red River basin. In contrast, the CV is only 14.7% for the Mackenzie  
374 River basin. The small  $S_b$  with its large interannual variations lead to the fact that years with  
375 large  $S_b$  often correspond to severe floods, and years with small  $S_b$  often correspond to very low  
376 flows, in the Red River (Wang and Russell, 2016). For the Mackenzie River basin, large and  
377 relatively stable snow amounts lead to the fact that the interannual variations of  $Q_{runoff}$  are very  
378 small and they are mainly determined by the temperature anomalies during the snowmelt season.  
379 The identification of major drivers for peak surface runoff for different basins is of importance in  
380 river flow modelling and flood forecasting.

381         The model performance for estimating peak river flow  $Q_{peak}$ , based on the above results  
382 for  $Q_{base}$  and  $Q_{runoff}$ , is shown in Table 3 and Fig. 4C. Compared to the mean observed  $Q_{peak}$  of  
383  $1.46 \text{ mm day}^{-1}$  ( $28,400 \text{ km}^3 \text{ s}^{-1}$ ) over the study period, the model result has a mean absolute error  
384 of  $MAE=0.1 \text{ mm day}^{-1}$  ( $1,878 \text{ km}^3 \text{ s}^{-1}$ ), or 6.5% of the mean  $Q_{peak}$  value. The modelled  $Q_{peak}$  for  
385 the 12 years has a correlation coefficient of  $r=0.83$  with the observed values at a significance  
386 level of  $p<0.001$ . The Nash–Sutcliffe model efficiency coefficient for peak river flow estimates  
387 is  $E=0.51$ . Of the peak river flow, 15% is contributed by baseflow and 85% by surface runoff. As  
388 such, the modelling accuracy in  $Q_{base}$  plays a small role in the modelling accuracy of peak river  
389 flows or flood forecasts. However, modelling accuracy for total winter baseflow ( $Q_{sum}$ ) could be  
390 of importance as  $Q_{sum}$  directly affects the estimate of  $S_b$  at spring break-up (Fig. 3), which is the  
391 case for the Red River basin. Compared to the dates for peak snowmelt, the dates for the peak  
392 river flow observed at the station had a delay varying from 13 to 41 days among the 12 years  
393 (Fig. 6). On average, the delay was  $\sim 22$  days. The hysteresis indicates the average travel time for  
394 the snowmelt water over the basin to reach the hydrometric station.



395 Results from the LOO-CV show that the 12 models trained using the 12 sets of n-1 (11  
396 years) samples all achieved a correlation coefficient of  $r > 0.8$  with the observed peak river flows  
397 at a significance level of  $p < 0.003$ , except for the run with year 2013 left-out which had a  $r = 0.71$   
398 and a significance level of  $p < 0.014$ . The model forecasts for peak river flows based on the 12  
399 models (Fig. 7) had a  $r = 0.72$  and  $MAE = 0.14 \text{ mm day}^{-1}$ , or 9.7% of the observed mean  $Q_{peak}$   
400 value. Compared with the model trained using data for all the years, the deterioration of the  
401 model performance in forecasting the peak river flows from LOO-CV reflects the limited  
402 number of data samples due to the short records of GRACE data. As the GRACE observations  
403 continue, and with the follow-up mission of GRACE-FO, it will be necessary to recalibrate the  
404 model to refine the parameter values and to increase the model robustness for peak river flow  
405 estimates and flood forecasting.

406 The impact of measurement and leakage error in the GRACE TWS on the model results  
407 was investigated by running the model with TWS adjusted by the error either at the pre-winter  
408 time (for baseflow) or at the spring breakup (for surface runoff). The impact of the TWS error on  
409 the peak river flow estimates was found to be mostly under  $MAE = 0.06 \text{ mm day}^{-1}$ , or 4% of the  
410 mean  $Q_{peak}$  value, which is substantially lower than the modelling error. Compared with that for  
411 the Red River basin, the impact of the GRACE TWS error on the modelling results is much  
412 smaller for the Mackenzie River basin. This is mainly due to the facts that for the Mackenzie  
413 River basin (1) the error in GRACE TWS is small (see Section 2) due to its large area and (2) the  
414 snow amount is much larger and the peak river flow is less sensitive to  $S_b$  than the Red River  
415 basin as discussed above.

416 The model showed a relatively lower correlation coefficient with observed peak flows for  
417 the Mackenzie River than that for the Red River (Wang and Russell, 2016). This is not surprising



418 as the Mackenzie River basin is huge and very complex in physiographic and climate conditions.  
419 Sub-basins in the Mackenzie River basin have varying flow regimes as detailed in Woo and  
420 Thorne (2003). For instance, most of the rivers in the southern basin and at low altitudes peak in  
421 early May, but in rivers at higher latitudes and high altitudes, where snowmelt is delayed, spring  
422 peaks occur later. In glacierized basins, the ablation of glaciers intensifies in the summer and  
423 this, together with snowmelt at high elevations, prolongs the high flows into summer. Large  
424 lakes and reservoirs are highly effective in providing large storage capacities to reduce high  
425 flows. The Mackenzie River, although it exhibits essentially a subarctic nival regime of  
426 snowmelt-induced peak flow, is a combination of many varying flow regimes of its sub-basins.  
427 Our model is a highly simplified representation of this complex system. In contrast, the  
428 physiographic and climate conditions for the Red River basin are much more monotonous.  
429 Secondly, the small interannual variations in snow amounts and peak flows of the Mackenzie  
430 River basin increase the impact of input data errors ( $Q$  and  $T_a$ ) on the model results and impose  
431 challenges on robust model calibration and validation.

432         Several water processes during the period from spring breakup to peak river flow, such as  
433 rain, evapotranspiration, soil thaw-induced surface infiltration or groundwater recharge, as well  
434 as lake storage and river ice dynamics, may significantly affect the magnitudes of peak river  
435 flows. The impacts of these processes are not explicitly included in the model and could be  
436 important sources in the modelling errors. In particular, substantial rain events over the snowmelt  
437 period can significantly affect peak river flows. The soil thaw-induced surface infiltration and  
438 groundwater recharge may have relatively small impacts, as the water flow is mainly from south  
439 to north and the lower river sub-basin is usually in a frozen state when the melted water from  
440 south arrives. Moreover, recharge of groundwater during this time period (if there is any) would



441 lead to an increase in baseflow, which offsets the impact of reduction in surface runoff due to  
442 infiltration of the snowmelt water. The calibration of the model using actual peak river flows also  
443 reduces the impact of this process on the peak river flow modelling. Nevertheless, explicitly  
444 including the above-mentioned water processes during the period from spring breakup to peak  
445 river flow in the model needs to be further studied.

446           One drawback of our method is that it does not recognise the spatial variations of snow  
447 amounts due to the large footprint of GRACE data. Consequently, the model cannot address the  
448 spatial snowmelt and water flow patterns within the basin which is expected to largely determine  
449 the hysteresis between peak snowmelt and peak river flows and to further reduce the modelling  
450 errors in peak flow forecasts. Nevertheless, as a case study with the available data and through  
451 comparison with the results from other basins, we have demonstrated encouraging results on  
452 peak river flow modelling and flood forecasting based only on GRACE TWS and temperature  
453 data. In practice, our GRACE-based method can be used in combination with other available  
454 data and methods to help improve the accuracy in peak flow or flood forecasts.

## 455 **5. Summary**

456           The peak river flow for the Mackenzie River is modelled in this study using GRACE  
457 satellite observations and temperature data, which advances the applications of space-based time-  
458 variable gravity measurements in cold region flood forecasting. The model estimates peak river  
459 flow by simulating peak surface runoff from snowmelt and the corresponding baseflow. The  
460 model closely estimated the observed values at a downstream hydrometric station. The results  
461 also revealed that on average the travel time for the snowmelt water to reach the hydrometric  
462 station is about 22 days. The major driver for determining the peak flow was found to be



463 atmospheric temperature variations. Compared with the Red River basin, the results highlight  
464 that the Mackenzie River basin has relatively high water storage and water discharge capability,  
465 and low snowmelt efficiency per unit temperature. Our GRACE-based approach for basin-scale  
466 snowfall estimation is independent of in situ measurements and largely eliminates the limitations  
467 and uncertainties present with traditional approaches. The results show that the GLDAS snowfall  
468 amount in our study region is about 20% lower than our GRACE-based estimate. The model is  
469 relatively simple and only needs data inputs of GRACE and atmospheric temperature  
470 observations for peak flow or flood forecasting. The model can be readily applied to other cold  
471 region basins, and could be particularly useful for regions with minimal data. In practice, this  
472 GRACE-based method can be used in combination with other available data and methods such  
473 as real-time flow data and flow routing models to help improve the accuracy in river flood  
474 forecasting, and develop reservoir operation procedures for flood and water resources  
475 management.

#### 476 **Acknowledgement**

477 This paper was internally reviewed by Dr. Aining Zhang and Don Raymond at Canada  
478 Centre for Mapping and Earth Observations. Comments are greatly appreciated. This study was  
479 supported by the Groundwater Geoscience Program and the Longterm Satellite Data Records  
480 project of the Earth Science Sector, Natural Resources Canada. GRACE land are available at  
481 <http://grace.jpl.nasa.gov>, supported by the NASA MEaSURES Program. The GLDAS data used  
482 in this study were acquired as part of the mission of NASA's Earth Science Division and  
483 archived and distributed by the Goddard Earth Sciences (GES) Data and Information Services  
484 Center (DISC).

485



486           **References:**

- 487    Andrews, J. 1993. Canada Water Book on Flooding. Environment Canada. Ottawa, Ontario.
- 488    B.C. Ministry of Forests, Lands and Natural Resource Operations, 2012. Flow Forecasting for  
489           the Lower Fraser River (from Hope to the Ocean). Prepared by: River Forecast Centre,  
490           Water Management Branch.
- 491    Burton, H., Rabito, F. Danielson, L., and Takaro, T. K. 2016. Health effects of flooding in  
492           Canada: A 2015 review and description of gaps in research. Canadian Water Resources  
493           Journal, 1-12. DOI: 10.1080/07011784.2015.1128854.
- 494    Church, M. 1974. Hydrology and permafrost with reference to northern North America.  
495           Proceedings, Workshop Seminar on Permafrost Hydrology. Ottawa: Canadian National  
496           Committee, International Hydrological Decade. 7–20.
- 497    Dong, J., Walker, J., and Houser, P. 2005. Factors affecting remotely sensed snow water  
498           equivalent uncertainty, Remote Sens. Environ., 97, 68–82, doi:10.1016/j.rse.2005.04.010.
- 499    Goodison B. E., Louie, P. Y. T., and Yang, D. 1998. WMO solid precipitation measurement  
500           intercomparison, WMO/TD 872, 212 pp., World Meteorol. Org., Geneva.
- 501    Griessinger, N., Seibert, J., Magnusson, J., and Jonas, T. 2016. Assessing the benefit of snow  
502           data assimilation for runoff modeling in alpine catchments. Hydrol. Earth Syst. Sci.  
503           Discuss., doi:10.5194/hess-2016-37.
- 504    Hall, D. K., Riggs, G. A., Salomonson, V. V., DiGirolamo, N. E., and Bayr, K. J. 2002. MODIS  
505           snow-cover products, Remote Sens. Environ., 83, 181–194.
- 506    Hall, D.K., Riggs, G.A., 2007. Accuracy assessment of the MODIS snow products. Hydrol.  
507           Process. 21, 1534–1547



- 508 International Joint Commission. 2000. Living with the Red, a Report to the Government of  
509 Canada and the United States on Reducing Flood Impacts in the Red River Basin. IJC:  
510 Ottawa and Washington; 273 pp.
- 511 Landerer, F. W. and Swenson, S. C. 2012. Accuracy of scaled GRACE terrestrial water storage  
512 estimates, *Water Resour. Res.*, 48, W04531, doi:10.1029/2011WR011453.
- 513 Li, L. and Simonovic, S. P. 2002. System dynamics model for predicting floods from snowmelt  
514 in North American prairie watersheds. *Hydrol. Process.* 16, 2645–2666. DOI:  
515 10.1002/hyp.1064.
- 516 Metcalfe, J.R, Ishida, S., and Goodison, B.E. 1994. A corrected precipitation archive for the  
517 Northwest Territories. Mackenzie Basin Impact Study Interim Report No. 2. Downsview,  
518 Ontario: Environment Canada. 110–117.
- 519 Nolin, A.W. 2010. Recent advances in remote sensing of seasonal snow. *Journal of Glaciology*,  
520 Vol. 56, 1141-1150.
- 521 Prowse, T., Shrestha, R. Bonsal, B. and Dibike Y. 2010, Changing spring air temperature  
522 gradients along large northern rivers: implications for severity of river-ice floods,  
523 *Geophysical Research Letters*, 37. 201-215.
- 524 Rannie, W. 2015. The 1997 flood event in the Red River basin: Causes, assessment and  
525 damages. *Canadian Water Resources Journal*, doi: 10.1080/07011784.2015.1004198
- 526 Swenson, S. C. and Wahr J. 2006. Post-processing removal of correlated errors in GRACE data.  
527 181 *Geophys. Res. Lett.* 2006;33 L08402.
- 528 Swenson, S. C. 2012. GRACE monthly land water mass grids NETCDF RELEASE 5.0. Ver.  
529 5.0. PO.DAAC, CA, USA. Dataset accessed 2015-11-30 at  
530 <http://dx.doi.org/10.5067/TELND-NC005>.





- 531 Wahr, J., Swenson, S., and Velicogna, I. 2006. Accuracy of GRACE mass estimates. *Geophys.*  
532 *Res. Lett.* 33, L06401.
- 533 Wang, S., Trishchenko, A. P., and Sun, X. 2007. Simulation of canopy radiation transfer and  
534 surface albedo in the EALCO model. *Climate Dynamics* 29:615–632. DOI  
535 10.1007/s00382-007-0252-y.
- 536 Wang, S. 2008. Simulation of evapotranspiration and its response to plant water and CO<sub>2</sub>  
537 transfer dynamics. *Journal of Hydrometeorology*, 9: 426-443. DOI:  
538 10.1175/2007JHM918.1.
- 539 Wang, S., Yang, Y., Luo, Y., and Rivera, A. 2013. Spatial and seasonal variations in  
540 evapotranspiration over Canada's landmass, *Hydrol. Earth Syst. Sci.*, 17, 3561–3575.  
541 doi:10.5194/hess-17-3561-2013.
- 542 Wang, S., McKenney, D. W., Shang, J., and Li, J. 2014a. A national-scale assessment of long-  
543 term water budget closures for Canada's watersheds, *J. Geophys. Res. Atmos.*, 119,  
544 8712–8725, doi:10.1002/2014JD021951.
- 545 Wang, S., Huang, J., Li, J., Rivera, A., McKenney, D.W., and Sheffield, J. 2014b. Assessment of  
546 water budget for sixteen large drainage basins in Canada. *J. Hydrology*, 512: 1-15,  
547 <http://dx.doi.org/10.1016/j.jhydrol.2014.02.058>.
- 548 Wang, S., Pan, M., Mu, Q., Shi, X., Mao, J., Brümmer, C., Jassal, R. S., Krishnan, P., Li, J., and  
549 Black, T. A. 2015a. Comparing evapotranspiration from eddy covariance measurements,  
550 water budgets, remote sensing, and land surface models over Canada. *J.*  
551 *Hydrometeorology*, 16: 1540-1560, doi: 10.1175/JHM-D-14-0189.1.



- 552 Wang, S., Huang, J. Yang, D. Pavlic, G. and Li, J. 2015b. Long-term water budget imbalances  
553 and error sources for cold region drainage basins. *Hydrological Processes*, 29, 2125–  
554 2136, doi: 10.1002/hyp.10343.
- 555 Wang, S. and Russell, H. 2016. Forecasting snowmelt-induced flooding using GRACE satellite  
556 data: A case study for the Red River watershed. *Canadian Journal of Remote Sensing* (in  
557 press).
- 558 Wang, S. and Li, J. 2016. Terrestrial water storage climatology for Canada from GRACE  
559 satellite observations in 2002–2014. *Canadian Journal of Remote Sensing* (in press).
- 560 Woo, M. K., Heron, R., Marsh, P., and Steer, P. 1983. Comparison of weather station snowfall  
561 with winter snow accumulation in High Arctic basins. *Atmosphere-Ocean* 21: 312–325.
- 562 Woo, M. K., and Thorne, R. 2003. Streamflow in the Mackenzie Basin, Canada, Arctic, 56, 328–  
563 340.
- 564 Yang, D., Kane, D., Zhang, Z., Legates, D., and Goodison, B. 2005. Bias-corrections of long-  
565 term (1973–2004) daily precipitation data over the northern regions. *Geophysical Research*  
566 *Letters* **32**: L19501, doi:10.1029/2005GL024057.
- 567 Yang, D., Shi, X., and Marsh, P. 2014. Variability and extreme of Mackenzie River daily  
568 discharge during 1973–2011, *Quatern Int*, doi:10.1016/j.quaint.2014.09.023.
- 569 Yang, D., Zhao, Y., Armstrong, R., and Robinsinon, D. 2009. Yukon River Streamflow Response  
570 to Seasonal Snowcover Changes, *Hydrol. Process.* 23, 109–121, DOI: 10.1002/7216.
- 571 Zhang, Y., Wang, S., Barr, A.G., and Black, T.A. 2008. Impact of snow cover on soil  
572 temperature and its simulation in the EALCO model. *Cold Regions Science and*  
573 *Technology*, 52, 355–370.
- 574



575 **Table 1. Baseflow model calibration and performance**

$a$ ( $\times 10^{-3} \text{ day}^{-1}$ )	$b$ (mm)	Correlation ( $r$ )	Significance ( $p <$ )	Average winter baseflow (mm)	Mean Absolute Error ( $MAE$ )		Nash–Sutcliffe model efficiency coefficient ( $E$ )
					(mm)	(%)	
1.07	-195.9	0.73	0.007	48.77	2.37	4.9%	0.53

576

577

578 **Table 2. Snowmelt model calibration and model performance for peak surface runoff**  
 579 **estimation**

$\alpha$ ( $\text{mm } ^\circ\text{C}^{-1}$ )	$\beta$ ( $^\circ\text{C}$ )	Correlation ( $r$ )	Significance ( $p <$ )	Average peak surface runoff ( $\text{mm day}^{-1}$ )	Mean Absolute Error ( $MAE$ )		Nash–Sutcliffe model efficiency coefficient ( $E$ )
					( $\text{mm day}^{-1}$ )	(%)	
17.0	2.1	0.82	0.001	1.26	0.10	7.6	0.50

580

581

582 **Table 3. Model performance for peak river flow estimation**

Correlation ( $r$ )	Significance ( $p <$ )	Average peak river flow ( $\text{mm day}^{-1}$ )	Mean Absolute Error ( $MAE$ )		Nash–Sutcliffe model efficiency coefficient ( $E$ )
			( $\text{mm day}^{-1}$ )	(%)	
0.83	0.001	1.46	0.1	6.5	0.51

583

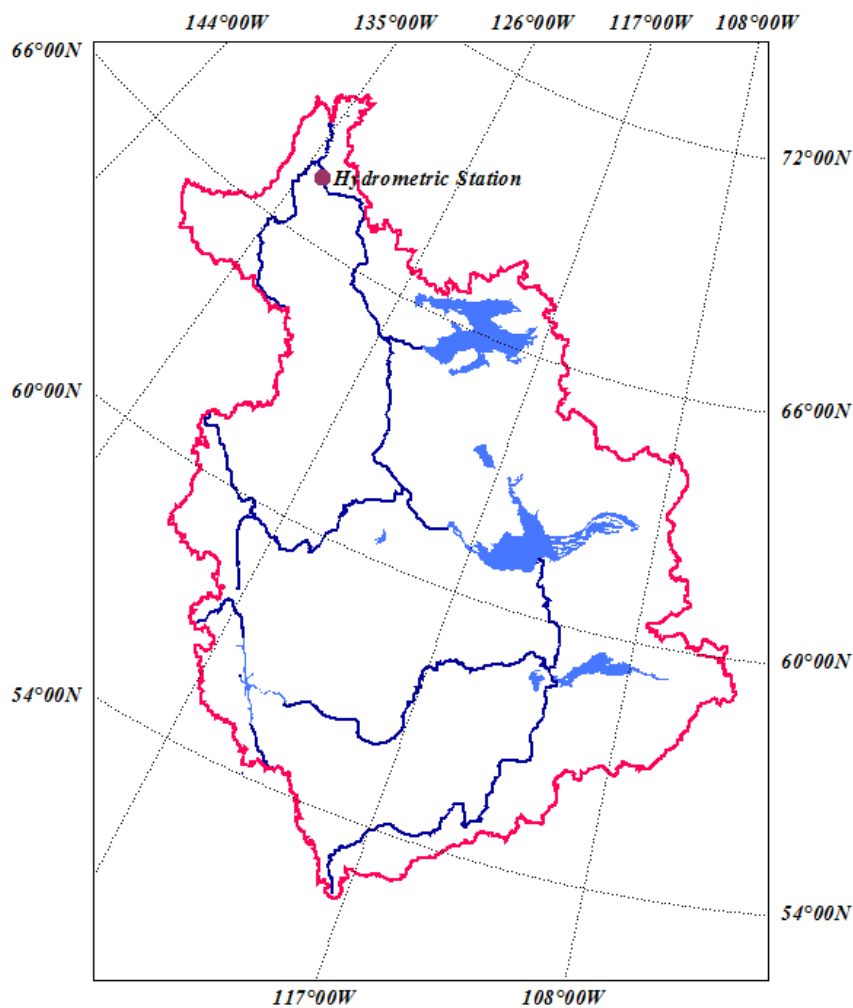
584



585 **Figure Captions:**

586

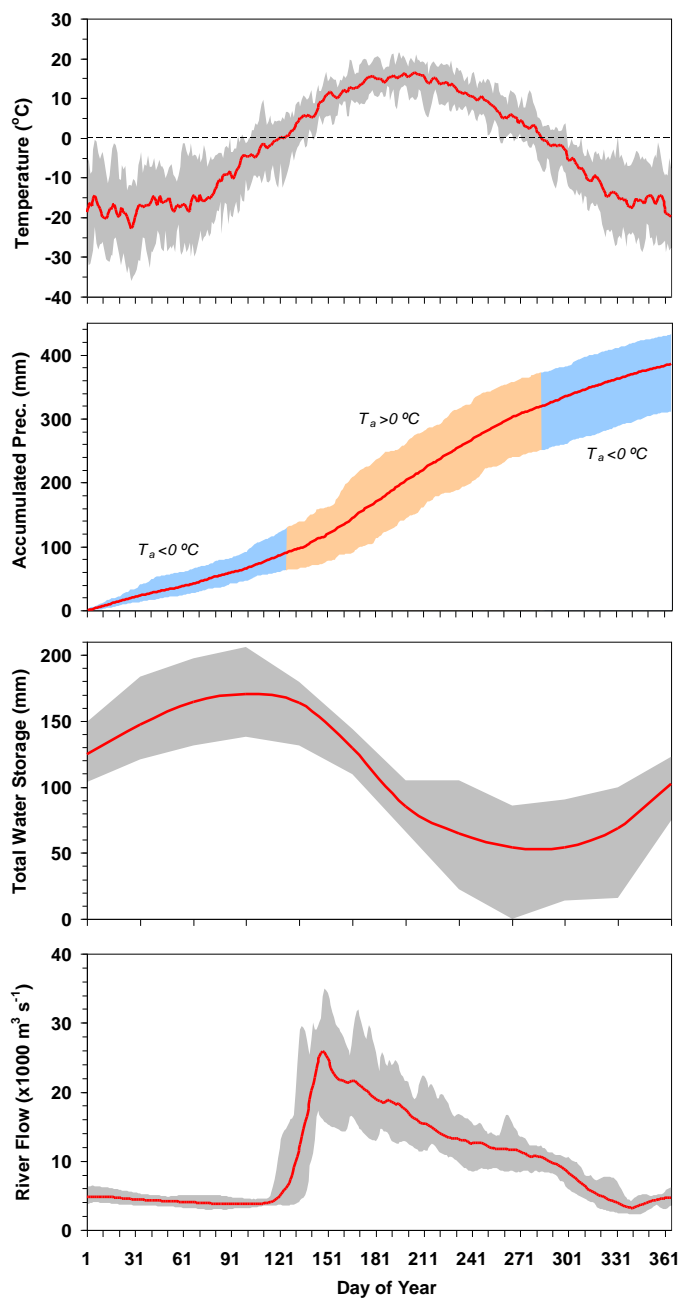
587



588

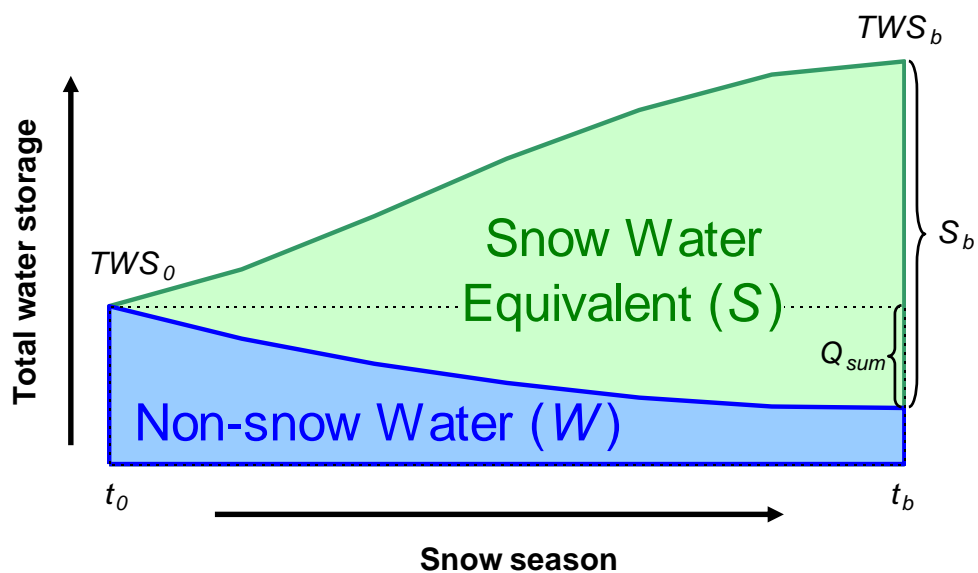
589 Figure 1. Map for the Mackenzie River basin and the hydrometric station used in this study.

590



591

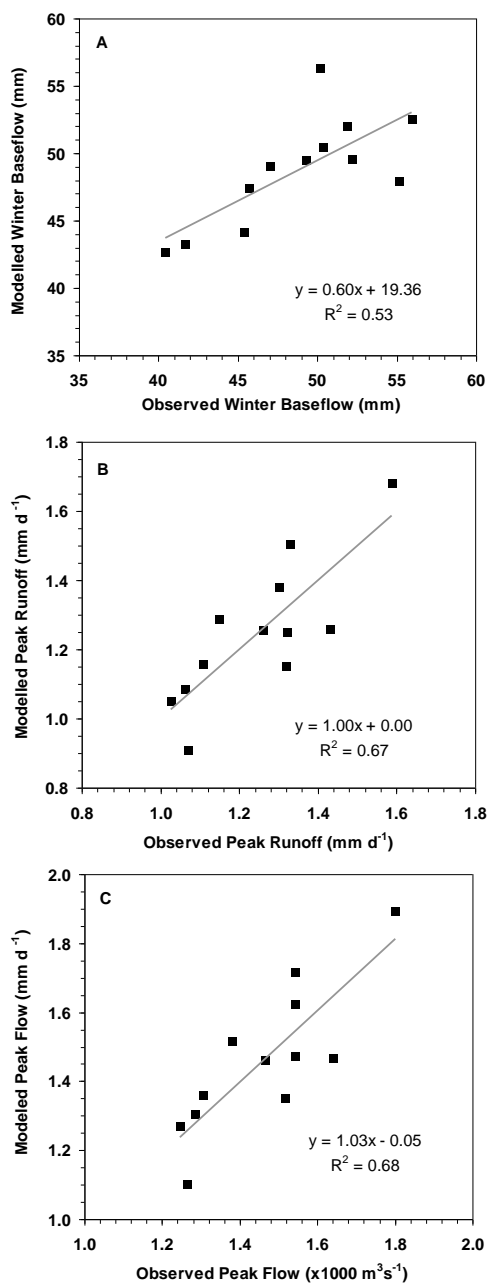
592 Figure 2. Hydroclimate characterization of the Mackenzie River basin (from top to bottom: air  
593 temperature, accumulated precipitation, total water storage change, and river flow. Lines  
594 represent the averages over the study period of 2002-2014. Shaded areas represent the  
595 maximum/minimum variation ranges).



596

597 Figure 3. Diagram showing snow accumulation and non-snow water storage change in winter. ( $t_0$   
598 and  $t_b$ : start and breakup of snow season;  $TWS_0$  and  $TWS_b$ : total water storage at  $t_0$  and  $t_b$ ;  $W$ :  
599 non-snow water;  $S_b$ : Snow Water Equivalent at  $t_b$ ;  $Q_{sum}$ : total river discharge in snow season).

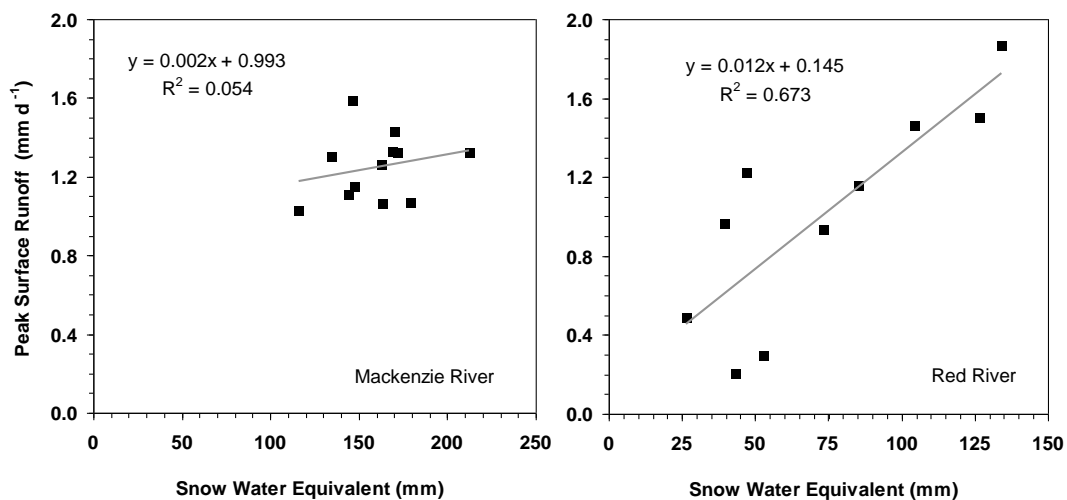
600



601

602 Figure 4. Comparisons of modelled vs. observed total baseflow in winter (A), peak surface  
603 runoff (B) and peak river flow (C).



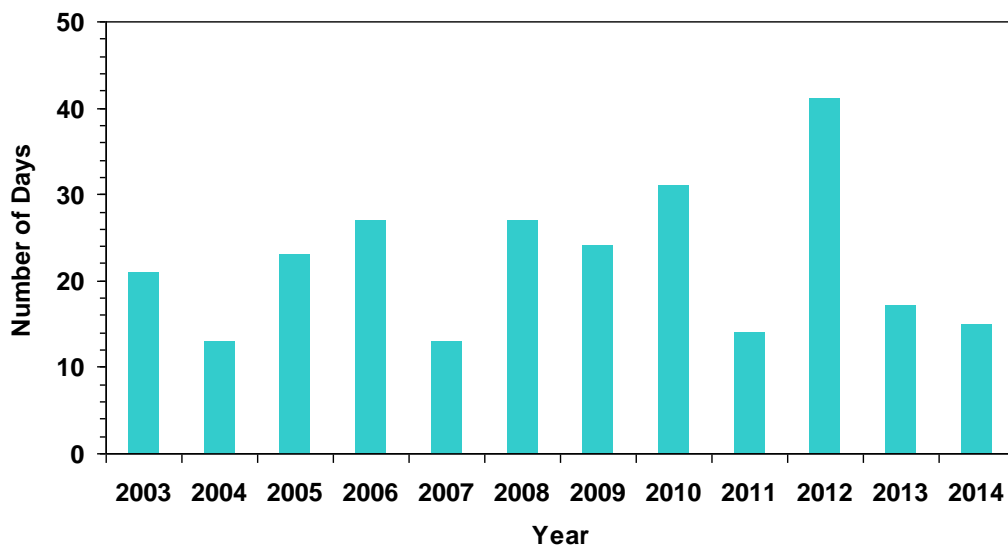


604

605 Figure 5. Peak surface runoff vs. snow water equivalent at spring break-up for the Mackenzie  
606 River basin (left) and the Red River basin (right).

607

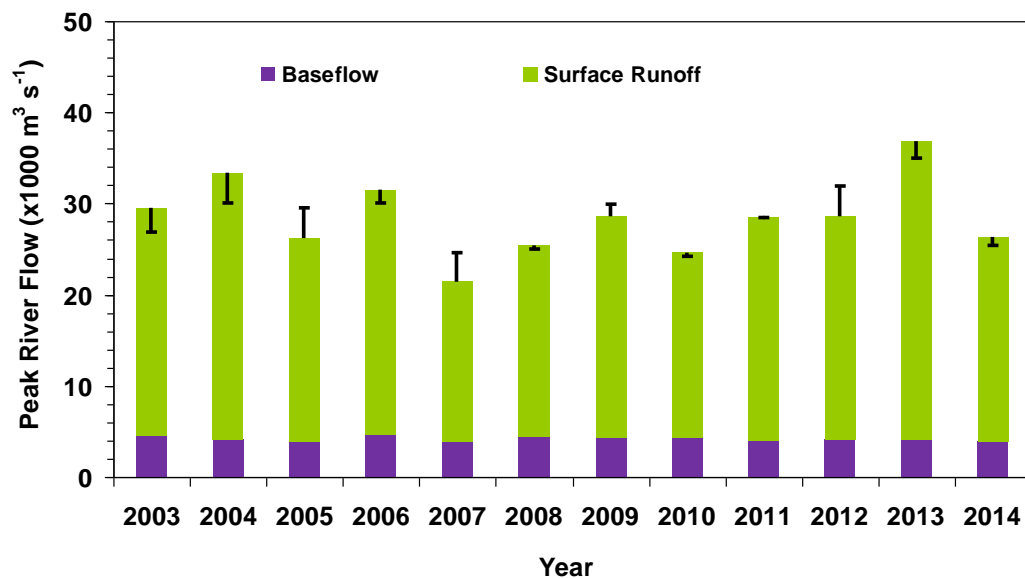
608



609

610 Figure 6. The travel time for snowmelt water from the basin to reach the hydrometric station.

611



612

613 Figure 7. The leave-one-out cross-validation (LOO-CV) modelling results for peak river flow

614 forecast. The error bar is the difference between forecasted and observed peak river flows.